



The Size Effect of SiO₂ Particles on Friction Mechanisms of a Composite Friction Material

Weitao Sun¹ · Wenlong Zhou¹ · Jianfa Liu¹ · Xuesong Fu¹ · Guoqing Chen¹ · Shan Yao¹

Received: 1 December 2017 / Accepted: 15 January 2018 / Published online: 25 January 2018
© Springer Science+Business Media, LLC, part of Springer Nature 2018

Abstract

In this paper, the effect of SiO₂ particle size on friction mechanisms was investigated. Five different size scales (10 μm, 80 μm, 180–700 μm, 700 μm–2.0 mm, and 3.0 mm) were selected to prepare non-commercial friction materials. Friction testing for these materials was conducted on a pad-on-disc-type friction tester under certain conditions. In order to identify the friction behaviour during the friction process, worn surfaces after test were observed using SEM. Results revealed that the friction mechanisms changed with particle size. In addition, a simple physical model was developed to provide quantitative analysis for the friction coefficient of materials containing large particles. Further, the predictability of this model was investigated across a range of formulations and controlling factors.

Keywords Particle size · Friction mechanisms · Friction materials · Physical model · Predictability

1 Introduction

Non-asbestos organic (NAO) friction materials have been widely used for many years in the braking field. This could be due to the fact that they comprise of diverse ingredients that can easily meet a wide range of requirements [1]. However, the application of NAO friction materials is seriously restricted by a common fade phenomenon induced by degradation of organic components at high temperatures [2, 3]. For the past few years, many efforts have been made to solve this problem [4–9]. Among these attempts, ceramic-enhanced NAO friction materials have attracted much attention owing to the suitable friction stability at high temperatures [10–15]. For this type of friction material, ceramic particles are usually designed as abrasives, and the tribology performance is highly dependent on the size of particles.

Many publications have researched the size effect of particles on the tribology performance of friction materials. For instance, Jang and his team investigated the size effect of zircon particles (1–150 μm) on friction stability, oscillation

of friction force, and wear resistance of brake linings [16]. The publication [12] studied the size effect of silicon carbide particles (3–40 μm) on the fade resistance and the formation of friction layer. In addition, Bijwe et al. even carried out a study on nano-abrasives [17]. Based on these studies, some conclusions were drawn suggesting that fine particles (smaller than 100 μm) usually work through a three-body abrasive mode, while coarse particles (larger than 150 μm) can develop into contact plateaus by themselves and usually work through a two-body abrasive mode.

However, it must be noted that the size scales of particles in these studies are not larger than 200 μm. In one study [11], though the size scale of particles reached 500 μm, these particles were external (not included in friction materials). Furthermore, most of these efforts were focused on the fade resistance, as well as the wear of materials and discs. Nevertheless, the size effect on friction mechanisms has been seldom studied.

In the present work, the size effect of SiO₂ particles on friction mechanisms was systematically investigated. Five non-commercial specimens containing particles with different size scales were prepared. Friction testing was conducted under constant speed, load, and temperature. The friction mechanisms as a function of particle size were studied by observing the worn surfaces. In addition, a simple physical model was firstly developed to provide a quantitative analysis for the friction coefficient of materials reinforced

✉ Xuesong Fu
xsfu@dlut.edu.cn

¹ Key Laboratory of Solidification Control and Digital Preparation Technology (Liaoning Province), School of Materials Science and Engineering, Dalian University of Technology, Dalian 116085, People's Republic of China

with large particles. The feasibility of the model across a range of formulations and operating conditions was verified through experiments.

2 Materials and Experiments

2.1 Preparation of Materials

Five different size scales of SiO₂ particles (10 μm, 80 μm, 180–700 μm, 700 μm–2.0 mm, and 3.0 mm) were selected to prepare non-commercial composite friction materials. The Vickers hardness of these particles is 8.32 GPa, and the density is 2.5 g/cm³. The composite friction materials consist of two components including resin matrix and particles. The volume fraction of particles is 36%. The composition of the resin matrix is given in Table 1. All of these ingredients except ceramic particles were firstly well mixed. The ceramic particles were then added into above mixture and well blended. Finally, the as-received mixture was moulded via hot-press according to a conventional process reported elsewhere [18]. Five composite materials— $P_{0.01}$, $P_{0.08}$, $P_{0.18-0.7}$, $P_{0.7-2.0}$, and $P_{3.0}$ —were prepared in the present study. They were reinforced with particles of 10 μm, 80 μm, 180–700 μm, 700 μm–2.0 mm, and 3.0 mm, respectively.

Table 1 Composition of the resin matrix in the composite materials (vol.%)

Category	Ingredient	Amount (%)
Binders	Phenolic resin	31.5
	Rubber	12.2
Reinforcement	Carbon fibres	10.5
Functional filler	Vermiculite	9.7
Space filler	Barite	32.5
Lubricant	Graphite	3.6

It should be noted that these composite materials investigated in this work were only designed for basic research. Disc wear, noise, and vibration caused by particles have attracted our attention, which will be discussed in other papers.

2.2 Experiments

Friction performance of the prepared materials was tested on JF 151 constant speed friction tester according to a non-standard procedure [19, 20]. The schematic diagrams of JF 151 friction tester and the non-standard test procedure are illustrated in Fig. 1. A grey iron disc with the nominal radius of 150 mm was employed as the counterdisc and could be rotated at a constant speed of 480 rpm by a motor. Before each test, two of the same specimens (Specimen 1 and Specimen 2, with a dimension of 25 mm × 25 mm × 6 mm) and the counterdisc were all scraped with 600# SiC paper. The test procedure involved two stages: a running-in stage and a test stage. Each stage was carried out for 5000 rotations. The running-in stage was performed to ensure a conformable contact for friction pairs. The temperature corresponding to this stage rose through friction heat and a heating device. The test stage was conducted at the constant temperature of 80 °C, constant rotating speed of 480 rpm, and constant load of 1225 N. The temperature was measured via a thermocouple on the disc and controlled through a heating device and an air blower.

Friction coefficient during the test stage was monitored. Following the test, worn surfaces of materials were observed through scanning electron microscopy (SEM, Zeiss SUPRA 55) to study the friction mechanisms.

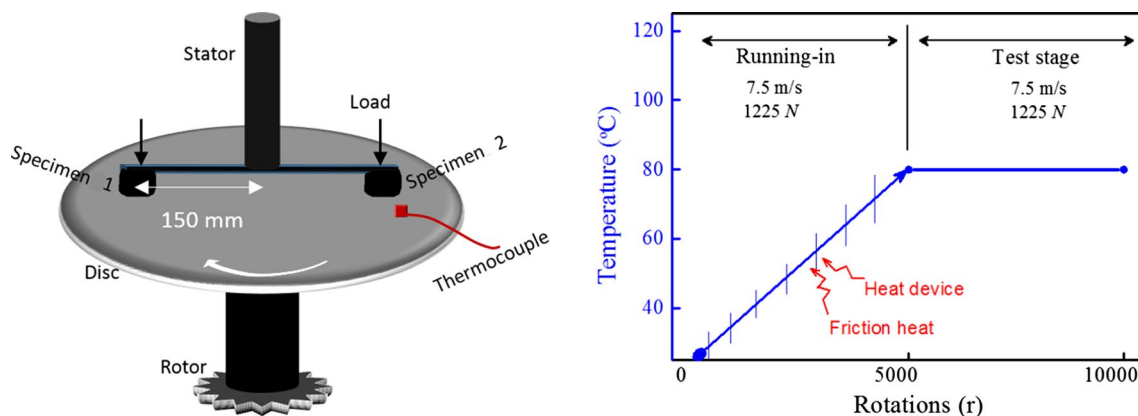


Fig. 1 Schematic diagrams of JF151 friction tester and the test procedure

3 Results and Discussion

The worn surfaces of different materials after test are exhibited in Fig. 2. It can be observed that the characteristic of worn surfaces changes with the particle size.

When the particles size is 10 μm , the worn surfaces are characterized by some contact plateaus (Fig. 2a). These plateaus were formed by compacted debris from both materials and discs under pressure and shear force [21]. Almost all of the friction behaviour happened on these plateaus. Thus, a conclusion can be drawn that particles of this size scale played an important role in the friction force by participating in the formation of plateaus.

As shown in Fig. 2b, many free particles can be observed on the very rough, worn surfaces of $P_{0.08}$. This was attributed to the fact that the particles of 80 μm were easily released from the resin matrix and arrested at the rubbing interface. As a result, some violent mechanical interactions between these particles and the friction pair could provide considerable resistance against the sliding. This is also known as the three-body abrasive mode [22, 23].

In Fig. 2c, the worn surfaces are characterized by some small pits and large contact plateaus. These pits were induced by the release of finer particles from the resin matrix, while these plateaus were formed by the larger particles themselves. The released finer particles at the rubbing interface could then contribute a lot to the friction

force with a three-body abrasive mode. The deformation resistance of the disc could resist against the sliding when the sharp edges or corners of the larger particles caused a plowing to the disc, which is known as a two-body abrasive mode [21]. Additionally, adhesive friction force could be generated on those plateaus. This is supported by the publications [22, 23], which held that adhesive friction always occurs at the clean rubbing interface through intermolecular force and develops an interfacial shear stress to resist against the sliding of friction couple.

When the particles size is 3 mm (Fig. 2d), these oversized particles are firmly embedded into the resin matrix and rise over the lowland. Furthermore, few pits or free particles can be observed on the surfaces. As compared to $P_{0.18-0.7}$, the friction for this material $P_{3.0}$ was dominated by the two-body abrasive mode and the adhesive friction.

The average friction coefficient during the test stage, as a function of particle size, is given in Fig. 3. It firstly increases and then decreases with the increasing particle size. This was determined by the roles of particles in the friction. Based on the above discussion, the transformation of friction mechanisms with particle size is illustrated in Fig. 3, and roughly divided into four regions. The fine particles of 10 μm worked through participating in the formation of contact plateaus. When the size was about 80 μm , the particles contributed a significant amount to the friction with a three-body abrasive mode. With the increase in particle size, a two-body abrasive mode and an adhesive friction occurred. Finally, when the size scale reached about 3.0 mm, the three-body

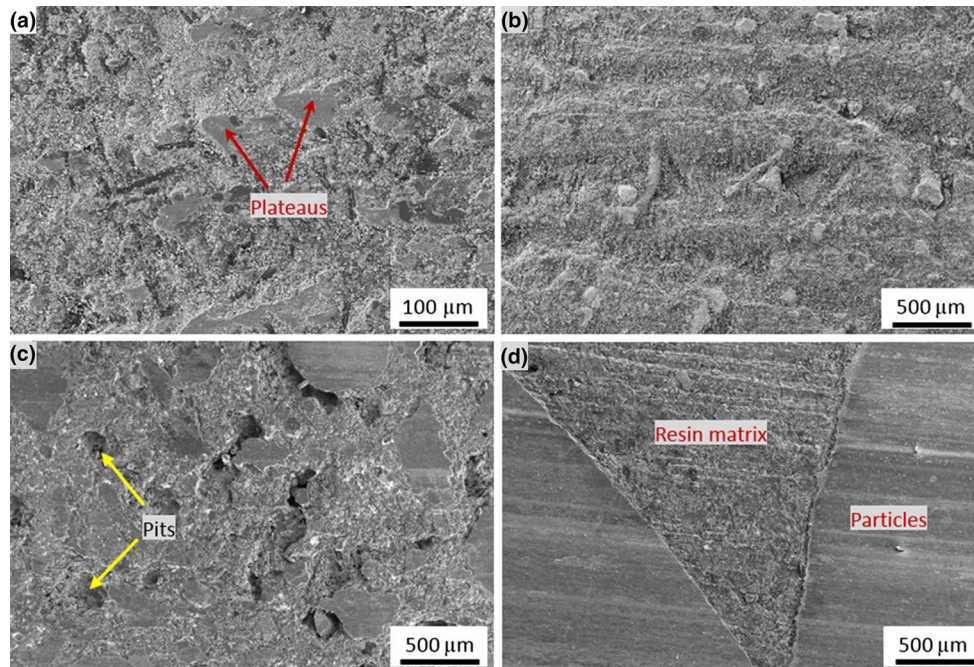


Fig. 2 Worn surfaces of different materials after test: **a** $P_{0.01}$; **b** $P_{0.08}$; **c** $P_{0.18-0.7}$; **d** $P_{3.0}$

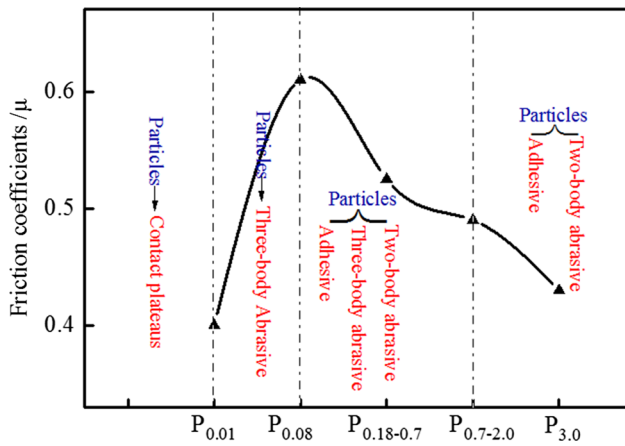


Fig. 3 Size effect of particles on the average friction coefficient and friction mechanisms

abrasive mode disappeared and was replaced by the adhesive friction and the two-body abrasive mode dominating the friction. Among these regions, the friction corresponding to the materials containing large particles ($P_{3.0}$) attracted our interest. Moreover, a simple model was established to give

a quantitative analysis for the friction corresponding to this region in the following section.

4 Establishment of Physical Model

According to the worn surfaces of $P_{3.0}$ (Fig. 2d), it can be concluded that the resin matrix was easily removed because of poor wear resistance and contributed little to the friction directly [24]. Simultaneously, the particles developed into the contact plateaus and carried most of the friction load. This special contact state is beneficial for quantitative analysis because many interference factors can be minimized or eliminated, such as the complicated interactions between the resin matrix and the disc, the complicated mechanical properties of different ingredients, and the heterogeneity of the resin matrix.

In order to establish the physical model of $P_{3.0}$, it is necessary to study the dynamic evolution of friction behaviour during the entire process. The morphology of particles before the running-in stage was measured by a 3D optical profiler characterized by many convex bodies, as shown in Fig. 4a. When the friction process reached a steady state,

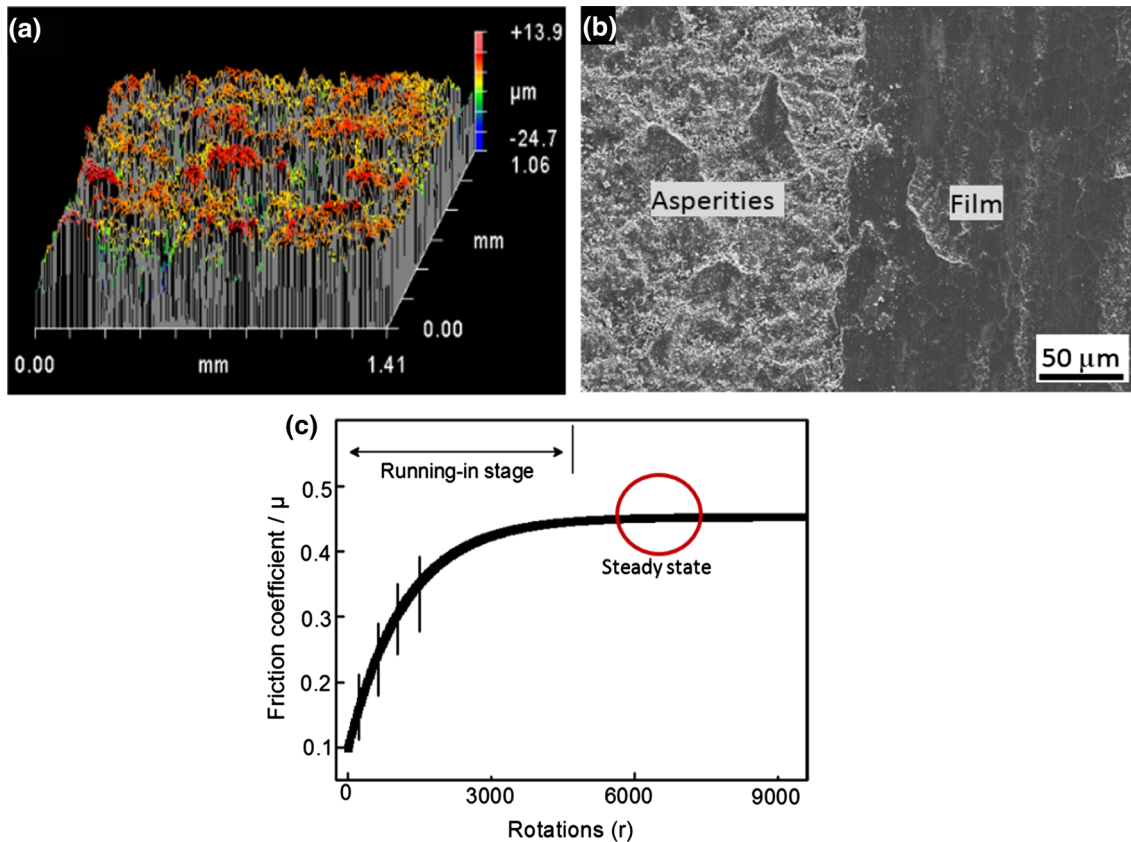


Fig. 4 **a** Morphology of particles before friction (scraped with 600# SiC paper); **b** the worn surfaces of particles corresponding to the steady state; **c** the schematic diagram of the entire friction process

parts of the surfaces are covered with smooth friction film, while the rest of the region is exposed (Fig. 4b). Therefore, the dynamic evolution of the friction behaviour can be deduced as follows. In the early stage, a mechanical plowing between these hard convex bodies and the softer disc dominated the friction process [23]. During this stage, the friction coefficient increased with sliding distance (Fig. 4c). As the friction process continued, the friction film formed by the compaction of debris was created on the surfaces of particles [21]. It should be noted that the destruction of friction film simultaneously happened owing to wear. When a balance between the destruction and formation of friction film was reached, a dynamic steady state was achieved, as marked by the red circle in Fig. 4c.

As discussed above, the friction force corresponding to the steady state was the contribution of two components, the two-body abrasive mode induced by the penetration of hard asperities into the softer disc, and the adhesive friction generated between the friction film and the disc through intermolecular force [22, 23]. Accordingly, a simple physical model was developed, and the geometric schematic is exhibited in Fig. 5. The model consists of three components including S_1 , S_2 , and S_3 , as shown by the top view. Here S_1 stands for the convex body located on the surface of particles, S_2 denotes the friction film created on the surface of particles, and S_3 refers to the resin matrix region. The specimens tested in this experiment contain m physical models in total. The sliding direction is marked with the blue arrow (Top view).

The geometry shape of S_1 is assumed as a rectangular pyramid, as shown by the front view in Fig. 5. The side length of base is a , the insertion depth into the disc is h , and the angle between two opposite faces is θ . When relative sliding happens, the deformation resistance of the disc resists against

the mechanical plowing caused by S_1 . The resistance can be expressed as:

$$F_1 = \frac{1}{2}ah\sigma, \tag{1}$$

where σ is the extrusion stress of the disc and can be replaced with the yield strength of the disc. This was enlightened by Kragel'Skii who proposed a spherical convex body inserted into the disc to model the behaviour of mechanical friction [25]. However, the model in the present paper is not plagiarized. This is owing to the fact that in the friction process, parameters and theoretical analysis are entirely different in the two cases.

With respect to S_2 , many adhesive junctions between the friction film and the disc are established through intermolecular force. During sliding process, these junctions can be destroyed under shear force and then re-established [23]. The resistance against the rupture of these junctions can be given as:

$$F_2 = S_2\tau, \tag{2}$$

where τ is the shear strength of these adhesive junctions, and S_2 is the area of the friction film in a model. For convenience, we define τ as the shear strength of the friction film.

Since almost the entire friction load was carried by the particles, the friction force induced by S_3 could be ignored.

The friction coefficient μ is calculated according to the classical law [26], as shown below.

$$\mu = \frac{F}{N} \tag{3}$$

The friction tester in the present work also used the law to collect the friction coefficient. Here F stands for the friction force of the specimens, and N is the load working on the specimens. F can be expressed as

$$F = (F_1 + F_2)m, \tag{4}$$

where m is the quantity of models in the specimens. Submitting Eqs. (1), (2), and (4) to Eq. (3), we obtain:

$$\mu = \frac{\left(\frac{1}{2}ah\sigma + S_2\tau\right)m}{N}. \tag{5}$$

In addition, the rubbing interface area S_0 of the specimens is given as:

$$S_0 = (S_1 + S_2 + S_3)m, \tag{6}$$

where S_1 , S_2 , and S_3 are the area of S_1 , S_2 , and S_3 , respectively. This is owing to the fact that S_1 and S_2 take up the whole worn surfaces of particles in each model, ω is introduced to describe the content of particles in the specimens, as shown.

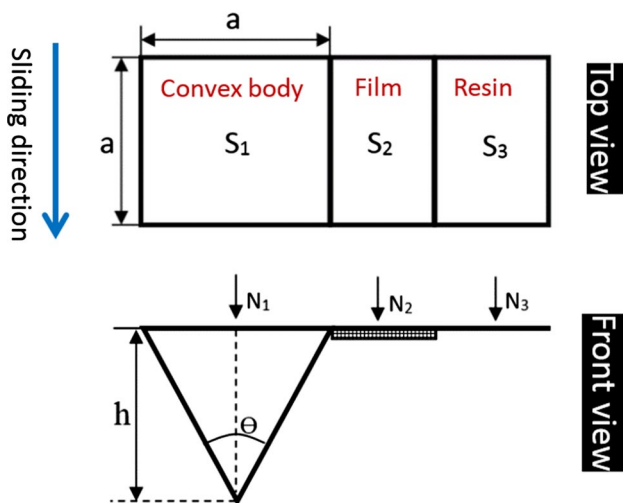


Fig. 5 Different views of the model: top view and front view

$$\omega = \frac{(S_1 + S_2)m}{S_0} \tag{7}$$

S_2 is obtained as:

$$S_2 = \frac{S_0\omega}{m} - S_1 \tag{8}$$

Since the insertion depth of convex into disc is mainly determined by the load N_1 working on S_1 and the yield strength σ of the disc, we can have:

$$N_1 = S_1\sigma \tag{9}$$

As discussed above (in Sect. 4, second paragraph), the convex bodies carried almost all of the load N before the formation of friction film. Thus the following equations can be obtained:

$$\frac{N}{m} = N_1 = S_1\sigma \tag{10}$$

$$N = S_1\sigma m \tag{11}$$

Submitting Eqs. (8) and (11) into Eq. (5), μ can be presented as:

$$\mu = \frac{\frac{1}{2}ah\sigma m}{S_1\sigma m} + \frac{\left(\frac{S_0\omega}{m} - S_1\right)\tau m}{N} \tag{12}$$

According to the geometry feature of the model, $h = \lambda a$, where λ is the geometry factor, Eq. (12) is simplified as:

$$\mu = \frac{\lambda}{2} + \frac{S_0\omega\tau}{N} - \frac{\tau}{\sigma} \tag{13}$$

where λ and S_0 are assumed as constants in this model, and friction coefficient μ is determined by ω , τ , N , and σ . The predictability of the model for τ , ω , and N will be discussed in the following section. This model is only established to provide a quantitative analysis for the friction of materials reinforced with large particles.

5 Predictability of Model

5.1 μ as a Function of ω

As described by Eq. (13), μ is deeply influenced by the content of particles ω . In order to obtain the experimental data concerning the effect of ω on μ , some specimens—S-1, S-2, S-3, S-4, and S-5—containing different contents of particles were prepared, as shown in Table 2. The resin matrix in each specimen has the same composition, which is given in Table 1.

Table 2 Content of particles in specimens

	Specimens				
	S-1	S-2	S-3	S-4	S-5
Ceramic particles (vol.%)	28.8	30.25	32.1	36.0	50.0
Resin matrix (vol.%)	71.2	69.75	67.9	64.0	50.0

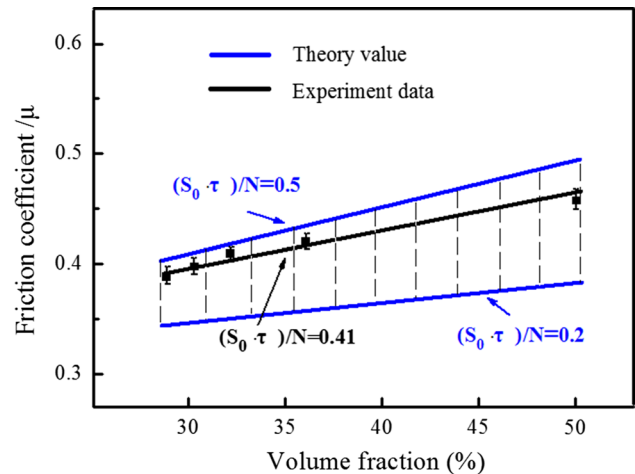


Fig. 6 Friction coefficient as a function of the content of particles (the two blue lines and the region between them are theoretical values, while the black line is experimental data) (Color figure online)

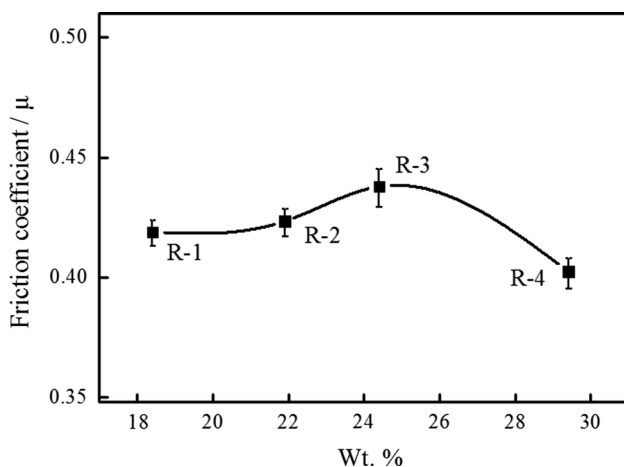
The friction testing was performed according to Sect. 2.2. The friction coefficient as a function of ω was collected and is plotted in Fig. 6. An approximate linear relationship between the friction coefficient μ and the content of particles ω is exhibited, and μ increases with the increase in ω , as shown by the black line in Fig. 6. The slope of the black line can be calculated through processing the experimental data, which is approximately 0.41. The intersection of the black line and X-axis is about 0.27.

According to the literature [25, 27], τ is in the range of 0.2–0.5 MPa corresponding to different metal–polymer friction pairs. The yield strength σ of disc used in the present work is much larger than τ , so $\frac{\tau}{\sigma}$ is assumed as zero. $\frac{N}{S_0}$ is 0.98 MPa, which has been demonstrated in Sect. 2.2. $\frac{\lambda}{2}$ is set as 0.27 by fitting the simulation result to the experimental data. Thus, the theoretical value of μ as a function of ω can be calculated according to Eq. (13), as shown by the two blue lines and the region between them. The slope of the theoretical line ranges from 0.2 to 0.5.

It can be seen that the model approximately meets the experimental data. The theoretical value is exhibited in a form of “range”, which is ascribed to an indetermination of the composition of friction film. Overall, a good predictability for the model to the experimental results is confirmed to some extent.

Table 3 Content of binders in the resin matrix of different specimens

Ingredient	Amount (wt.%)			
	R-1	R-2	R-3	R-4
Phenolic resin (modified by rubber)	18.4	21.9	24.4	29.4
Carbon fibres	3.1	3.1	3.1	3.1
Vermiculite	3.1	3.1	3.1	3.1
Barite	49.1	45.6	43.1	38.1
Graphite	1.8	1.8	1.8	1.8
Wollastonite	24.5	24.5	24.5	24.5

**Fig. 7** Friction coefficient as a function of the content of binders in the resin matrix

5.2 μ as a Function of τ

As described by Eq. (13), friction coefficient μ is highly dependent on the shear strength of friction film τ . Friction film is usually generated by the compaction of wear debris from both materials and disc at the rubbing interface [21]. As such, the microstructure and properties of friction film are determined by the materials formulation.

In the present section, we primarily planned to change the shear strength of friction film τ through changing the content of binders in composite friction materials. This is because binders are very important ingredients exerting a significant impact on τ . Some specimens—R-1, R-2, R-3, and R-4—with different contents of binders were prepared and are shown in Table 3. The mass fraction vacancy was balanced by barite, which is always designed as space filler [2]. The volume fraction of particles in every specimen remained constant (36%).

The friction coefficient of these specimens was also tested according to the procedure described in Sect. 2.2, and the results are given in Fig. 7. It can be seen that the friction coefficient increases firstly and then decreases with the

increase in binders. Subsequently, in order to build the correlation between μ and τ , the morphology of friction film created on particles was observed through SEM, and the photographs are exhibited in Fig. 8.

As shown in Fig. 8a1 and a2, the friction film generated on particles in specimen R-1 is characterized by a loose and discontinuous structure. This may be explained by the lesser amount of binders, which resulted in a poorer compaction of wear debris. This is in agreement with the publication [21], which held that binders, temperature, and pressure are important for the formation of friction film. As a consequence, the loose friction film could be easily destroyed without enough shear strength during a friction process. The friction film corresponding to R-3 is more compact, as shown in Fig. 8b1 and b2. Further, the failure mechanism of this film was dominated by peeling off of sheet film. Therefore, the conclusion can be drawn that the shear strength of the film corresponding to R-3 is higher when compared to R-1. With respect to the friction film of R-4 (Fig. 8c1, c2), the film is very compact and uniform, but characterized by obvious plastic deformation. The great plasticity induced by increasing binders was responsible for poorer shear strength of film. Thus, it can be concluded that the shear strength of friction film corresponding to R-3 is higher than that of both R-1 and R-4. This conclusion is consistent with the experimental results in Fig. 7. Accordingly, a suitable predictability for the model to the experimental results is indirectly verified.

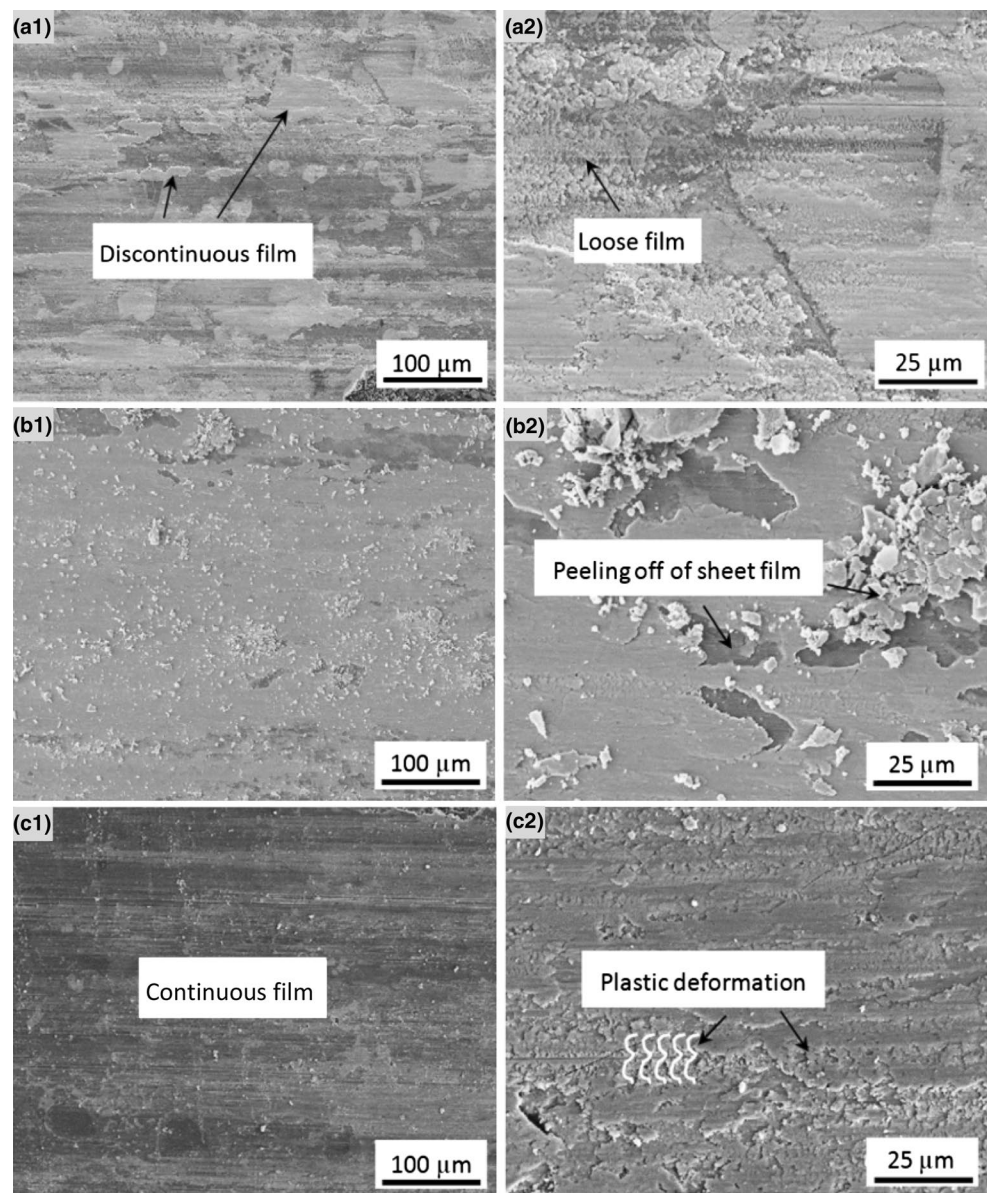
5.3 μ as a Function of N

The effect of load N on friction coefficient has been reported by many publications. As reported by the literature [22, 28], friction coefficient decreases with the rise of load. Because of the uniqueness of this type of composite friction material investigated in our present work, it is necessary to verify the predictability for the model to the effect of load on μ through experiments.

Specimen S-4 described in Table 2 was employed in the present section. Friction coefficient as a function of load was tested. Four loads (1225 N, 1102.5 N, 857.5 N, and 612.5 N) were used in the present section, while other conditions remained the same as Sect. 2.2. The experimental results are plotted with a black curve in Fig. 9. It can be observed that the friction coefficient decreases with the increase in load.

For the model, ω corresponding to specimen S-4 is 36%, which is described in Table 2. To fit the simulation results to the experimental data, τ and $\frac{\lambda}{2}$ are assumed as 0.41 MPa and 0.27, respectively, which has been obtained in Sect. 5.1. S_0 is 1250 mm², which is calculated according to the dimension of the specimens. Submitting these parameters to Eq. (13), the value of $S_0\omega\tau$ is obtained as 184.5 N, and the theoretical μ as a function of N can be obtained (blue line in Fig. 9).

Fig. 8 Morphology of friction film created on particles in R-1: **a1** $\times 500$, **a2** $\times 2000$; morphology of friction film created on particles in R-3: **b1** $\times 500$, **b2** $\times 2000$; morphology of friction film created on particles in R-4: **c1** $\times 500$, **c2** $\times 2000$



The value of $S_0\omega\tau$ for the black line is about 196 N, which is calculated by processing the experimental results.

It can be understood that the experimental results are highly consistent with the theoretical curve. Consequently, a good predictability for the model to the effect of N on μ is confirmed. The various loads that can have an effect on τ in practice may explain the deviation.

6 Conclusion

In the present paper, five different size scales of particles were employed to enhance one non-commercial friction material. The friction mechanisms under moderate testing conditions were researched. The results indicated that particle size has a significant influence on the transformation of friction mechanisms.

1. When the size was smaller than 10 μm , particles contributed a lot to the friction force by participating in the formation of contact plateaus.

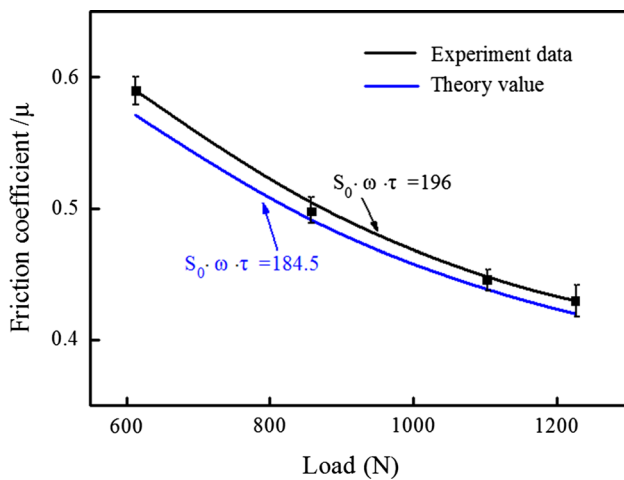


Fig. 9 Friction coefficient as a function of load

- When the size reached about 80 μm , particles worked with a three-body abrasive mode.
- When the size was in the range of 180 μm –2 mm, particles contributed a lot to the friction force with three modes: the two-body abrasive mode, the three-body abrasive mode, and the adhesive friction.
- When the size reached about 3.0 mm, particles carried almost the entire friction load with the two-body abrasive mode and the adhesive friction.

In addition, a simple physical model was developed to provide a quantitative analysis for the friction of material reinforced with large particles. As described by the model, the friction coefficient is dependent on the content of particles, the shear strength of friction film, and load. The feasibility of the model was confirmed through experiments.

Acknowledgements This work was supported by the National High Technology Research and Development Program (“863” Program) of China under grant number SS2015AA042502.

References

- Cho, M.H., Kim, S.J., Kim, D., Jang, H.: Effects of ingredients on tribological characteristics of a brake lining: an experimental case study. *Wear* **258**, 1682–1687 (2005)
- Nidhi, M., J. Bijwe, Mazumdar, N.: Influence of amount and modification of resin on fade and recovery behavior of non-asbestos organic (NAO) friction materials. *Tribol. Lett.* **23**, 215–222 (2006)
- Bijwe, J., Nidhi, M., Majumdar, N., Satapathy, B.K.: Influence of modified phenolic resins on the fade and recovery behavior of friction materials. *Wear* **259**, 1068–1078 (2005)
- Singh, T., Patnaik, A., Chauhan, R., Rishiraj, A.: Assessment of braking performance of lapinus–wollastonite fibre reinforced friction composite materials. *J. King Saud Univ. Eng. Sci.* **29**, 183–190 (2017)
- Zhu, Z.C., Xu, L., Chen, G.A.: Effect of different whiskers on the physical and tribological properties of non-metallic friction materials. *Mater. Des.* **32**, 54–61 (2011)
- Öztürk, B., Arslan, F., Öztürk, S.: Effects of different kinds of fibres on mechanical and tribological properties of brake friction materials. *Tribol. Trans.* **56**, 536–545 (2013)
- Zhao, G., Hussainova, I., Antonov, M., Wang, Q.H., Wang, T.M.: Friction and wear of fiber reinforced polyimide composites. *Wear* **301**, 122–129 (2013)
- Baklouti, M., Cristol, A.L., Desplanques, Y., Elleuch, R.: Impact of the glass fibers addition on tribological behavior and braking performances of organic matrix composites for brake lining. *Wear* **330–331**, 507–514 (2015)
- Hee, K.W., Filip, P.: Performance of ceramic enhanced phenolic matrix brake lining materials for automotive brake linings. *Wear* **259**, 1088–1096 (2005)
- Boz, M., Kurt, A.: The effect of Al_2O_3 on the friction performance of automotive brake friction materials. *Tribol. Int.* **40**, 1161–1169 (2007)
- Hamid, M.K.A., Stachowiak, G.W., Syahrullail, S.: The effect of external grit particle size on friction coefficients and grit embedment of brake friction material. *Procedia Eng.* **68**, 7–11 (2013)
- Matějka, V., Lu, Y.F., Jiao, L., Huang, L., Martynková, G.S.: Effects of silicon carbide particle sizes on friction-wear properties of friction composites designed for car brake lining applications. *Tribol. Int.* **43**, 144–151 (2010)
- Ma, Y.N., Martynková, G.S., Valášková, M., Matějka, V., Lu, Y.F.: Effects of ZrSiO_4 in non-metallic brake friction materials on friction performance. *Tribol. Int.* **41**, 166–174 (2008)
- Shin, M.W., Kim, H., Jang, H.: Effect of the abrasive size on the friction effectiveness and instability of brake friction materials: a case study with Zircon. *Tribol. Lett.* **55**, 371–379 (2014)
- Lee, E.J., Hwang, H.J., Lee, W.G., Cho, K.H., Jang, H.: Morphology and toughness of abrasive particles and their effects on the friction and wear of friction materials: a case study with zircon and quartz. *Tribol. Lett.* **37**, 637–644 (2010)
- Cho, K.H., Jang, H., Hong, Y.S., Kim, S.J., Basch, R.H., Fash, J.W.: The size effect of zircon particles on the friction characteristics of brake lining materials. *Wear* **264**, 291–297 (2008)
- Bijwe, J., Aranganathan, N., Sharma, S., Dureja, N., Kumar, R.: Nano-abrasives in friction materials-influence on tribological properties. *Wear* **296**, 693–701 (2012)
- Ertan, R., Yavuz, N.: An experimental study on the effects of manufacturing parameters on the tribological properties of brake lining materials. *Wear* **268**, 1524–1532 (2010)
- Wang, Z.H., Hou, G.H., Yang, Z.R., Jiang, Q., Zhang, F., Xie, M.H., Yao, Z.J.: Influence of slag weight fraction on mechanical, thermal and tribological properties of polymer based friction materials. *Mater. Des.* **90**, 76–83 (2016)
- Wang, F.H., Liu, Y.: Mechanical and tribological properties of ceramic-matrix friction materials with steel fiber and mullite fiber. *Mater. Des.* **57**, 449–455 (2014)
- Eriksson, M., Lord, J., Jacobson, S.: Wear and contact conditions of brake pads: dynamical in situ studies of pad on glass. *Wear* **249**, 272–278 (2001)
- Saffar, A., Shojaei, A.: Effect of rubber component on the performance of brake friction materials. *Wear* **274–275**, 286–297 (2012)
- Glaseser, W.A.: *Characterization of Tribological Materials*. Harbin Institute of Technology Press, Harbin (2014)
- Eriksson, M., Jacobson, S.: Tribological surfaces of organic brake pads. *Tribol. Int.* **33**, 817–827 (2000)
- Kragel’skiĭ, V.I., Kombatov, V.S., Dobyichin, M.N.: *Friction and Wear Calculation Methods*. Pergamon Press, New York (1982)

26. Blau, P.J.: The significance and use of the friction coefficient. *Tribol. Int.* **34**, 585–591 (2001)
27. Briscoe, B., Scruton, B., Willis, F.R.: The shear strength of thin lubricant films. *Proc. R. Soc. Lond. Ser. A* **333**, 99–114 (1973)
28. Gopal, P., Dharani, L.R., Blum, F.D.: Load, speed and temperature sensitivities of a carbon-fiber reinforced phenolic friction material. *Wear* **181–183**, 913–921 (1995)